Phase transition and electrical studies of wolframium doped SrBi$_2$Ta$_2$O$_9$ ferroelectric ceramics

Indrani Coondoo · A. K. Jha · S. K. Agarwal · N. C. Soni

Abstract In this study, crystalline structure, dielectric and impedance properties of SrBi$_2$Ta$_2$O$_9$ (SBT) - based ferroelectric ceramics have been investigated with the substitution of wolframium/tungsten (W) onto the tantalum site. Wolframium doped SrBi$_2$(W$_x$Ta$_{1-x}$)$_2$O$_9$ (0.0 ≤ x ≤ 0.20) ceramics were synthesized by solid state reaction method. The X-ray diffractogram analysis revealed that the substitution formed a single phase layered perovskite structure for the doping content up to x ≤ 0.05. The dielectric measurements as a function of temperature show an increase in Curie temperature (T$_c$) over the composition range of x = 0.05 to 0.20. The W^{6+} substitution in perovskite-like units results in a sharp dielectric anomaly at the ferroelectric phase transition. Furthermore, the dielectric constant at their respective Curie temperature increases with wolframium doping. Both enhanced Curie temperatures and dielectric constants at the Curie points indicate an increase in polarizability, which could be attributed to the increased "rattling space" due to the incorporation of the smaller tungsten cations. The dielectric loss reduces significantly with tungsten addition. AC impedance properties vis-à-vis wolframium content has also been studied.

Keywords Aurivillius · Dielectric properties · Strontium bismuth tantalate · Impedance analysis

I. Coondoo · A. K. Jha (✉)
Department of Applied Physics, Delhi College of Engineering,
Delhi-110042, India
e-mail: akj6467@indiatimes.com

S. K. Agarwal · N. C. Soni
National Physical Laboratory, Dr. K. S. Krishnan Road, New Delhi-110012, India

1 Introduction

The family of mixed bismuth oxides with general formula [Bi$_2$O$_2$]$^{2+}$[A$_{n-1}$B$_n$O$_{3n+1}$]$^{2-}$ was first studied by Aurivillius [1–4]. Their structures comprise intergrowths of [Bi$_2$O$_2$]$^{2+}$ layers with perovskite [A$_{n-1}$B$_n$O$_{3n+1}$]$^{2-}$ layers (n = 1, 2, 3, 4). Among the bismuth layered structure ferroelectrics (BLSFs), SrBi$_2$Ta$_2$O$_9$ (SBT), SrBi$_2$Nb$_2$O$_9$ (SBN) and their solid solutions are the best candidates for application in information data storage such as ferroelectric random access memories (FeRAMs). They offer several advantages, being lead-free, fatigue—free and having independence of ferroelectric properties with film thickness, as compared with isotropic perovskite ferroelectrics such as Lead Zirconium Titanate (PZT) [5–7].

Understanding of these perovskite ferroelectric materials in respect of their *A*- and *B*- site substitutions, which affects their physical and chemical properties is known. This effect has been extensively exploited in piezoelectrics and ferroelectrics to improve their performance [8–14]. Most of the research effort on the improvement of the dielectric and ferroelectric properties are based on the *A*-site substitutions in SBT. However, the authors could find only limited work on the dielectric and ferroelectric properties of the layered perovskite, SBT, through substitution of the *B*-site ions (Ta^{5+}) with other alternate cations of higher oxidation state. Various doping ions, such as La^{3+}, Nd^{3+} and Nb^{5+} in PZT result in enhanced remnant polarization and a decreased coercive field [15–16]. Similar results were obtained in SBN ferroelectric ceramics through partial substitution of Nb^{5+} by V^{5+} [17, 18]. Thus doping SBT with smaller wolframium (W^{6+}) for tantalum (Ta^{5+}) could be an approach for improving the dielectric and ferroelectric properties of SBT.

In this paper, we present the effects of substitution of wolframium for tantalum, on the structural, dielectric and impedance properties of SrBi$_2$Ta$_2$O$_9$ferroelectric ceramics.

2 Experimental

Ceramic samples with compositions SrBi$_2$(W$_x$Ta$_{1-x}$)$_2$O$_9$ (SBWT), with x ranging from 0.0 to 0.2 were synthesized by the solid-state reaction method taking SrCO$_3$, Bi$_2$O$_3$, Ta$_2$O$_5$ and WO$_3$ (all from Aldrich) in their stoichiometric proportions. The powder mixtures were thoroughly ground, passed through a sieve of appropriate size and then calcined at 900°C–1050°C in air for 2 h. The calcined mixtures were ground and admixed with about 1–1.5 wt% polyvinyl alcohol (Aldrich) as a binder and then pressed at ∼300 MPa into disk shaped pellets. The pellets were sintered at 1150°C for 2 h in air.

X-ray diffractograms of both the calcined and sintered samples were recorded using a Bruker diffractometer in the range 10° ≤ 2θ ≤ 70° with CuK$_α$ radiation at a scanning rate of 0.05°/second. The sintered pellets were polished to a thickness of ∼1 mm and coated with silver paste on both the sides for use as electrodes and cured at 550°C for half an hour. The dielectric and impedance measurements were carried out using a Solartron-1260 Impedance/gain–phase analyzer operating at oscillation amplitude of 1 V. The dielectric constant as a function of temperature was measured at a frequency of 100 kHz while the impedance measurements were carried out in the frequency range 10 to 10^6 Hz.

3 Results and discussion

3.1 XRD analysis

Figure 1 shows the XRD patterns of the various SBWT sintered samples. It is observed that the single phase layered perovskite structure is formed in the range 0.0 ≤ x ≤ 0.05. For the doped compositions with x > 0.05, in addition to the major peaks representing the layered perovskite phase, an unidentified peak is also observed. It seems that this peak could be possibly due to some unreacted tungsten oxide.

The diffraction patterns were indexed as belonging to the space group A2$_1$am [19]. Sixteen diffraction peaks were used for calculating and refinement of the lattice parameters using a least square refinement method, by means of a computer program package- Powdin [20]. The lattice parameters were used to calculate structural distortion parameters such as tetragonal strain (c/a) and orthorhombic distortion (b/a).

On the basis of ionic radii of atoms and coordination number(Table 1), it is expected that the tungsten ions will occupy tantalum (B) sites. Moreover, due to a smaller ionic radius
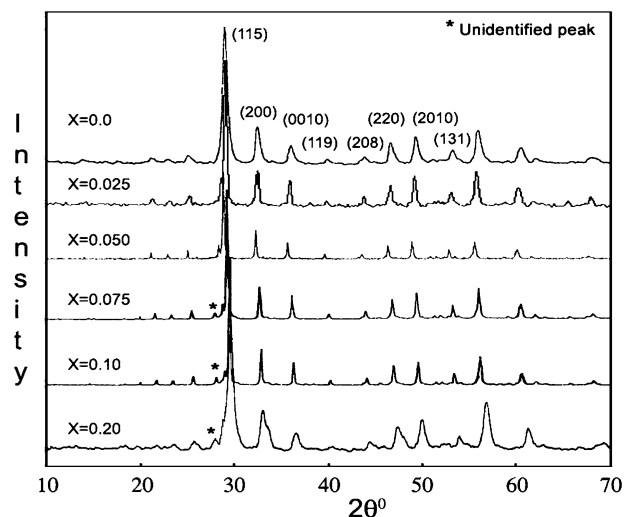
Fig. 1 XRD patterns of SrBi$_2$(W$_x$Ta$_{1-x}$)$_2$O$_9$ sintered at 1150°C

of W^{6+} than that of Ta^{5+}, decrease in the lattice constants is expected. As expected, the lattice parameters (Table 1) decrease with increasing concentration of tungsten. The variation of tetragonal strain as a function of concentration of tungsten is shown in Fig. 3.

3.2 Dielectric properties

Figure 2 shows the dielectric constants (Fig. 2(a)) and dielectric loss (Fig. 2(b)) as a function of temperature for doped and undoped ceramics measured at a frequency of 100 kHz with oscillating amplitude of 1 V. For all the samples, there is a sharp transition in dielectric constant at their respective Curie temperature, T_c where dielectric constant is a maximum. The dielectric measurements as a function of temperature show that the T_c decreases from ≈328°C (for x = 0.0) to ≈302°C (for x = 0.025) while over the composition range of x = 0.05 to 0.20, the T_c shows an increasing trend.

In the donor doped SBT, because of the constraint of maintaining the overall charge neutrality of the structure, substitution of W^{6+} ions for Ta^{5+} should result in the formation of cation vacancies, possibly at the A-site. The defect chemical reaction could be simplified as following:

Table 1 Elements in most stable valence state with their ionic radius (IR)[21] and coordination number (CN). Lattice parameters a, b and c of SrBi$_2$(W$_x$Ta$_{1-x}$)$_2$O$_9$ ceramics

Ions	IR (Å)	CN	x	a(Å)	b(Å)	c(Å)
Sr^{2+}	1.44	12	0.0	5.5243	5.5337	25.1001
Bi^{3+}	0.96	5	0.025	5.5215	5.5090	24.9767
Ta^{5+}	0.64	6	0.050	5.5172	5.5062	25.0046
W^{6+}	0.60	6	0.075	5.5005	5.4807	25.0156
			0.100	5.4822	5.4689	25.0354
			0.200	5.4852	5.4628	25.0701
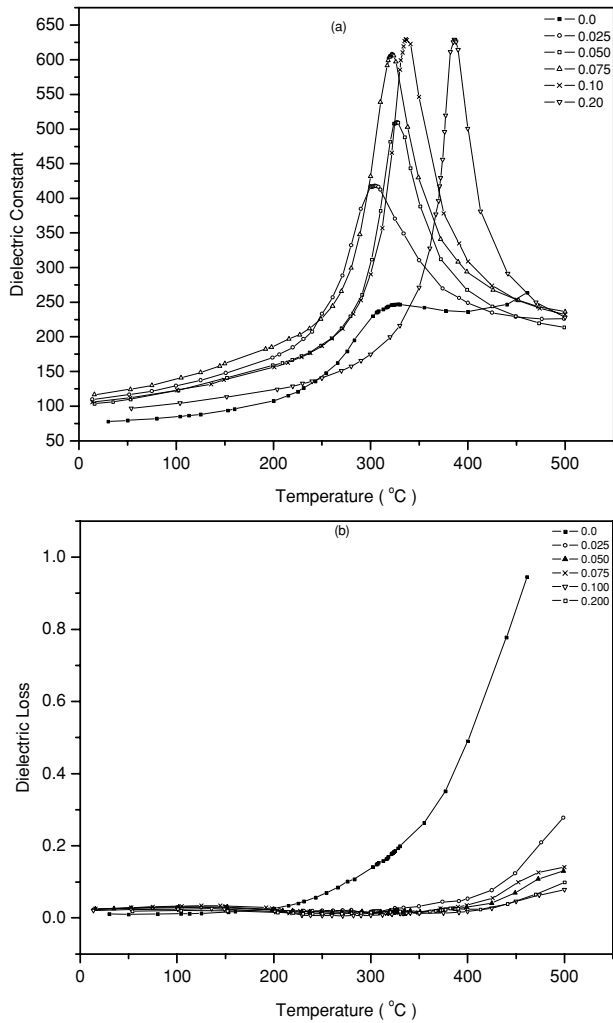
Fig. 2 (a) Dielectric constant and (b) Dielectric loss of SrBi$_2$ (W$_x$Ta$_{1-x}$)$_2$O$_9$ samples as a function of temperature at 100 kHz

$$Null = W^{.}_{Ta} + \frac{1}{2} V''_{Sr} \qquad (1)$$

where V_{sr} denotes the strontium vacant site. When the dopant concentration is low, the introduction of cation vacancies at the A site could possibly have resulted in an increase in the internal localised stress making the perovskite structure less stable thereby decreasing the T_c. For higher concentrations of tungsten a significant lattice distortion is evident from the large decrease in the values of lattice parameters *a* and *b* (Table 1). Hence, because of the decrease in unit cell volume and the introduction of cation vacancies at the *A*-site, the perovskite-like unit is likely to be under compressive stress. This leads to an enhancement of ferroelectric structural distortion, thus resulting in a higher T_c [22]. Another explanation of such behavior of T_c with composition can be studied in terms of the tetragonal strain. Tetragonal strain is the internal strain in the lattice which affects the phase transition temperature in the structure [15]. Large value of strain corresponds
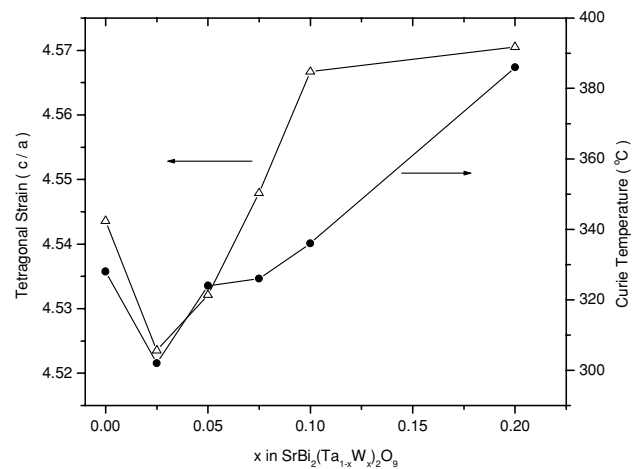
Fig. 3 Tetragonal strain and Curie temperature as a function of concentration of tungsten in SrBi$_2$(W$_x$Ta$_{1-x}$)$_2$O$_9$

to greater amount of thermal energy required to carry out the phase transition and therefore an increase in T_c is expected with an increase in the strain. The variation of tetragonal strain and Curie temperature as a function of tungsten in SrBi$_2$(W$_x$Ta$_{1-x}$)$_2$O$_9$ is shown in Fig. 3. The T_c decreases for $x = 0.025$ and then increases for higher concentrations of tungsten. Similar trend is also observed in the variation of tetragonal strain (Fig. 3) as a function of tungsten concentration. Thus the observed change in Curie temperature may also be attributed to the change in tetragonal lattice strain.

Figure 2(b) shows the dielectric loss (at 100 kHz) as a function of temperature for SBT doped with various amounts of tungsten. It is observed that tungsten doping reduces the dielectric loss in the doped SBT ceramics. It is possibly due to the formation of cationic vacancies that effectively suppress the formation of oxygen vacancies and decreases the contribution of such space charges and, thus, a decrease in dielectric loss of doped SBT ceramics is observed [23–24].

In Fig. 4 it is observed that the peak dielectric constant at the Curie temperature, T_c, increases with the doping concentration. It is known that a shift in T_c to a higher temperature corresponds to an increased polarizability, which can be explained by the enlarged "rattling space" [25]. In addition, the incorporation of tungsten ions into the SBT structure is likely to introduce some cationic vacancies, so as to maintain the electrical neutrality. These cationic vacancies generated by donor doping make domain motion easier and increase the dielectric permittivity [24, 26]. Thus an increase in dielectric constant is observed.

3.3 Impedance analysis

Complex impedance spectroscopy (CIS) is a well-known and powerful technique for investigating the electrical and dielectric properties of materials [27]. The a.c. technique of CIS
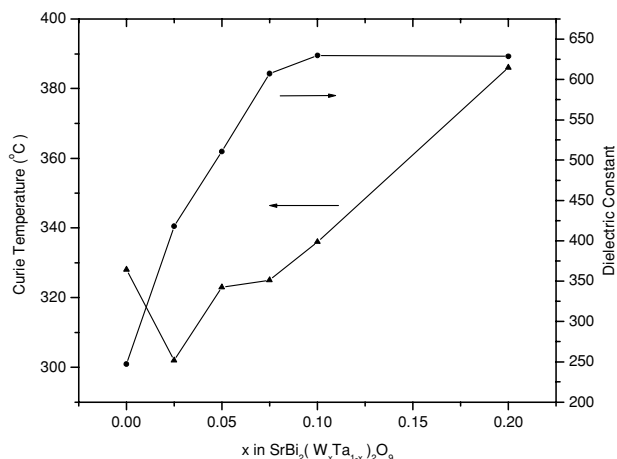
Fig. 4 The variation of Curie temperature and dielectric constant at T_c versus concentration of tungsten in $SrBi_2(W_xTa_{1-x})_2O_9$. The solid lines drawn are only guide to the eye

Table 2 Bulk resistance (R_b), grain boundary resistance (R_{gb}), bulk capacitance (C_b) and bulk conductivity (σ_b) of $SrBi_2(W_xTa_{1-x})_2O_9$ ceramics

x	$R_b(\Omega)$	$R_{gb}(\Omega)$	$C_b(pF)$	$\sigma_b \times 10^{-7}$ $(\Omega\ cm)^{-1}$
0.0	2.7×10^4	0.615×10^4	775	27.741
0.025	5.3×10^5	–	401	1.5623
0.050	9.64×10^5	–	452	0.6380
0.075	2.45×10^5	–	365	2.9061
0.100	1.16×10^6	–	433	0.6390
0.200	2.5×10^6	–	612	0.3368

enables us to evaluate and separate the contribution to the overall electrical properties, of the various components such as bulk, grain—boundary or polarization phenomenon in a material, in the frequency or time domain [28]. It is based on the principle of analyzing the a.c. response of a cell to a sinusoidal electrical signal and subsequent calculation of the resulting transfer function (impedance) with respect to the frequency of the applied signal. The electrical response recorded at the output, when compared with the sinusoidal input signal applied across the cell, provides us the impedance modulus $|Z|$ and phase shift (θ). The experimental output response so obtained, when depicted in a complex plane plot, appears in the form of a succession of semicircles/arcs in the frequency domain, arising as a result of the contribution to the electrical properties due to various components such as the bulk material, the grain boundary effects and interfacial polarization phenomenon (at the material-electrode interface).

Figure 5 shows the complex impedance plane plots of the $SrBi_2(W_xTa_{1-x})_2O_9$ ceramics for different concentrations of tungsten at 425°C. For undoped SBT, the Z' vs Z'' curve is composed of two semicircles, a large one and a small one (Fig. 5(a)). The large semicircle at high frequencies indicates the effect of the grain and the small one at low frequencies reflects the grain boundary contribution. The Z'-Z'' plots of doped SBT samples are dominated by a single semicircle. The predominant semicircle represents the impedance contribution of the grains indicating that the grain boundaries have a less significant contribution to the impedance in the case of doped SBT ceramics. The values of R_b, C_b, σ_b of the ceramics are listed in Table 2. The value of bulk resistance (R_b; contribution from the grain interior) is found by the low frequency intercept of the first semicircle on the real axis. The semicircle passes through a maximum at a frequency f_o (re-

laxation frequency) and satisfies the condition $2\pi f_o R_b C_b = 1$ where C_b is the bulk capacitance (capacitance of the grain interior). The value of bulk conductivity, σ_b is calculated by the equation:

$$\sigma_b = \left(\frac{1}{Z'}\right)\left(\frac{t}{A}\right) \qquad (2)$$

where Z' is the real part of the impedance (intersection of semicircle on the real axis), t is the thickness and A is the area of the sample.

It is observed (Table 2) that with increase in tungsten concentration, the bulk resistance increases and the bulk conductivity decreases. The oxygen vacancies are considered to be the most mobile ionic charge carriers in the perovskite oxides [29]. The high conductivity value of $x = 0.0$ sample can be attributed to the presence of oxygen vacancies due to the Bi_2O_3 volatilization during sintering. In doped SBT, to achieve charge neutrality, the substitution of W^{6+} onto Ta^{5+} would be accompanied by the formation of cation vacancies and subsequent elimination of oxygen vacancies resulting in a significant decrease of vacancy complexes formed due to Bi_2O_3 volatilization. It is the decrease in the concentrations of the oxygen vacancies that a decrease in conductivity with increasing concentration of tungsten is observed. Moreover, the increase in the lattice strain for higher concentration of tungsten (Fig. 3) which is responsible for trapping of electrons inside the domains [30], might be responsible for the decrease in the bulk conductivity values.

4 Conclusions

It is concluded from the present work that the single phase layered perovskite structure is maintained up to $x \approx 0.05$ in $SrBi_2(W_xTa_{1-x})_2O_9$ (SBWT). The Curie temperature decreased from ≈ 328°C for SBT to ≈ 302°C for SBWT with tungsten content, $x = 0.025$; thereafter an upward trend is
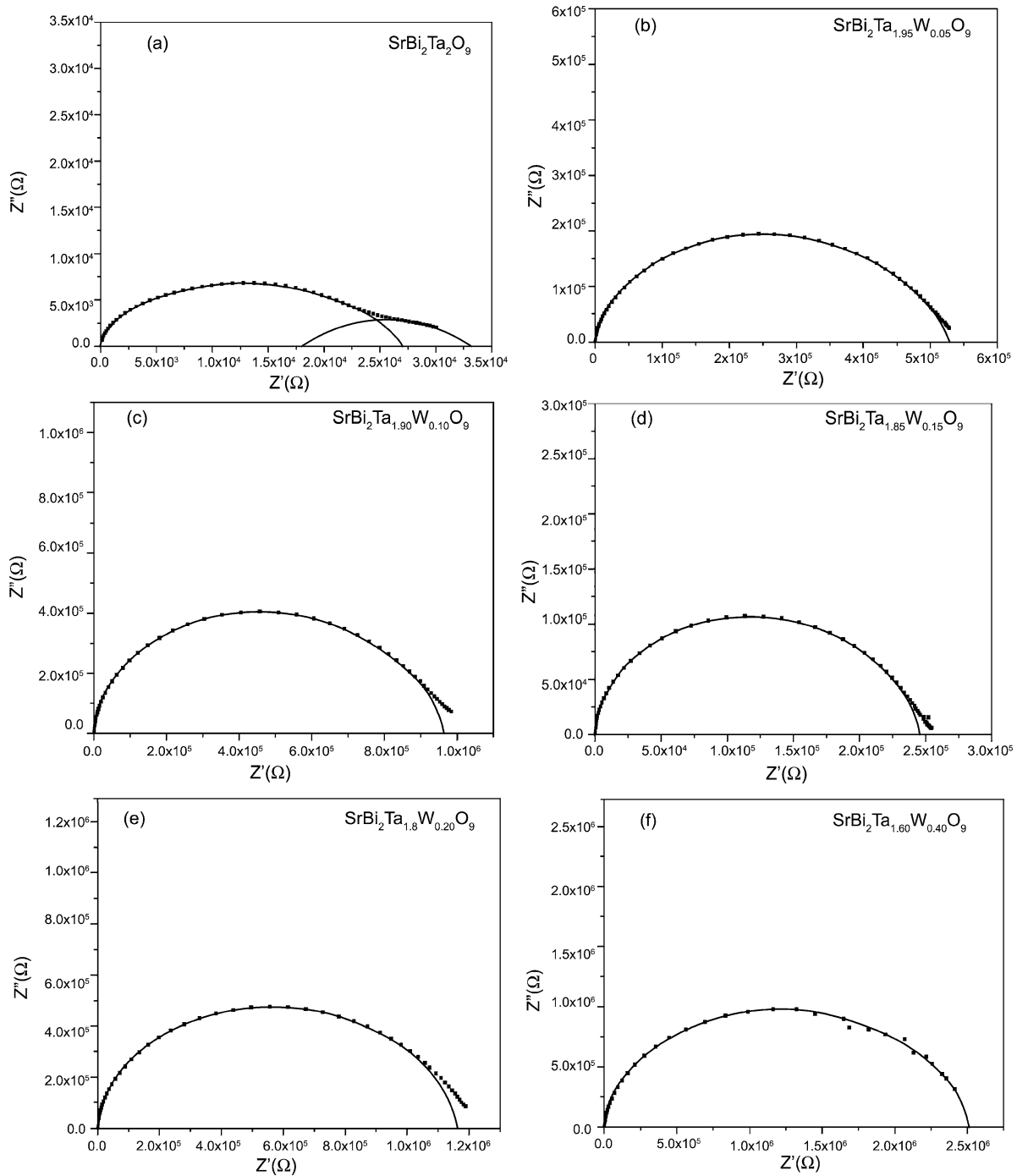
Fig. 5 Complex impedance plane plots at 425°C for (a) $x = 0.0$, (b) $x = 0.025$, (c) $x = 0.050$, (d) $x = 0.075$, (e) $x = 0.10$, (f) $x = 0.20$ in $SrBi_2(W_x Ta_{1-x})_2 O_9$

observed in the values of Curie temperature with tungsten concentration. The peak dielectric constant at the Curie temperature is found to increase with increasing concentration of tungsten. The dielectric loss reduces significantly on the introduction of tungsten into the parent structure, SBT. Doping SBT with cations of the higher oxidation state such as W^{6+} for Ta^{5+}, may result in enhanced remnant polarization

and decreased coercive field, and might become a promising material for FeRAMs.

References

1. B. Aurivillius, *Ark. Kemi*, **1**, 463 (1949).
2. B. Aurivillius, *Ark. Kemi*, **1**, 499 (1949).
3. B. Aurivillius, *Ark. Kemi*, **2**, 519 (1950).
4. B. Aurivillius, *Ark. Kemi*, **5**, 39 (1952).
5. J.F. Scott and C.A. Paz de Araujo, *Science*, **246**, 1400 (1989).
6. T. Mihara, H. Yoshimori, H. Watanabe, and C.A.P. Araujo, *Jpn. J. Appl. Phys.*, **34**, 5233 (1995).
7. C.A.P. De Araujo, J.D. Cuchlaro, L.D. McMillan, M.C. Scott, and J.F. Scott, *Nature*, **374**, 627 (1995).
8. F. Kulcsar, *J. Amer. Ceram. Soc.*, **42**, 343 (1959).
9. R.B. Atkin, R.L. Holman, and R.M. Fulrath, *J. Amer. Ceram. Soc.*, **54**, 113 (1971).
10. P. Duran-Martin, A. Castro, P. Millan, and B. Jimenez, *J. Mater. Res.*, **13**, 2565 (1998).
11. P. Millan, A. Ramirez, and A. Castro, *J. Mater. Sci. Lett.*, **14**, 1657 (1995).
12. T. Atsuki, N. Soyama, T. Yonezawa, and K. Ogi, *Jpn. J. Appl. Phys.*, **34**, 5096 (1972).
13. M.J. Forbess, S. Seraji, Y. Wu, C.P. Nguyen, and G.Z. Cao, *Appl. Phys. Lett.*, **76**, 2934 (2000).
14. E.C. Subbarao, *J. Phys. Chem. Solids*, **23**, 665 (1962).
15. Y.H. Xu, *Ferroelectric Materials and their Applications* (Elsevier Science Publishers, Amsterdam, 1991) p. 131.
16. R.B. Atkin and R.M. Fulrath, *J. Amer. Ceram. Soc.*, **54**, 265 (1971).
17. Y. Wu and G.Z. Cao, *Appl. Phys. Lett.*, **75**, 2650 (1999).
18. Y. Wu, G.Z. Cao, *J. Mater. Res.*, **15**, 1583 (2000).
19. Y. Noguchi, M. Miyayama, and T. Kudo, *Phys. Rev.*, **B63**, 214102 (2001).
20. E.Wu, POWD, An interactive powder diffraction data interpretation and indexing program Ver2.1, School of Physical Science, Flinders University of South Australia, Bedford Park S.A. JO42AU.
21. R.D. Shannon , *Acta. Crystallogr.*, **B25**, 925 (1965).
22. Y. Wu, C. Nguyen, S. Seraji, M.J. Forbess, S.J. Limmer, T. Chou, and G. Cao, *J. Ame. Ceram. Soc.*, **84**, 2882 (2001).
23. Y. Noguchi and M. Miyayama, *Appl. Phys. Lett.*, **78**, 1903 (2001).
24. Y. Wu, S.J. Limmer, T.P. Chou, and C. Nguyen, *J. Mater. Sci. Lett.*, **21**, 947 (2002).
25. K. Singh, D.K. Bopardikar, and D.V. Atkare, *Ferroelectrics*, **82**, 55 (1988).
26. S. Takahashi and M. Takahashi, *Jpn. J. Appl. Phys.*, **11**, 31 (1972).
27. J.R. MacDonald, *Impedance Spectroscopy* (Wiley, New York, 1987).
28. T.C. Chen, C.L. Thio, and S.B. Desu, *J. Mater. Res.*, **12**, 2628 (1997).
29. D.M. Smyth, *Ferroelectrics*, **116**, 117 (1991).
30. N.A. Schmidt, *Ferroelectrics*, **31**, 105 (1981).